© 2015. Published by The Company of Biologists Ltd | The Journal of Experimental Biology (2015) 218, 1393-1401 doi:10.1242/jeb.106914

RESEARCH ARTICLE

The descent of ant: field-measured performance of gliding ants

Yonatan Munk[1,2,*], Stephen P. Yanoviak[3], M. A. R. Koehl[2] and Robert Dudley[2,4]

ABSTRACT

Gliding ants avoid predatory attacks and potentially mortal consequences of dislodgement from rainforest canopy substrates by directing their aerial descent towards nearby tree trunks. The ecologically relevant measure of performance for gliding ants is the ratio of net horizontal to vertical distance traveled over the course of a gliding trajectory, or glide index. To study variation in glide index, we measured three-dimensional trajectories of *Cephalotes atratus* ants gliding in natural rainforest habitats. We determined that righting phase duration, glide angle, and path directness all significantly influence variation in glide index. Unsuccessful landing attempts result in the ant bouncing off its target and being forced to make a second landing attempt. Our results indicate that ants are not passive gliders and that they exert active control over the aerodynamic forces they experience during their descent, despite their apparent lack of specialized control surfaces.

KEY WORDS: Aerodynamics, Arboreal ants, Rainforest, Biomechanics, Particle filter

INTRODUCTION

All gliding animals control the trajectory of their descent while falling through air by converting gravitational potential energy into useful aerodynamic work and generating a controlled horizontal velocity component (Dudley et al., 2007). Vertebrates comprise the majority of described gliders, with examples including flying squirrels, snakes, frogs and lizards (Bahlman et al., 2013; Bishop, 2006; Emerson and Koehl, 1990; McCay, 2001; McGuire, 2003; McGuire and Dudley, 2005; Socha et al., 2005; Young et al., 2002). In terrestrial invertebrates, although gliding performance has been suggested as a selective factor in the evolution of wings in early insects (Kingsolver and Koehl, 1994), gliding was unknown until the recent discovery of directed aerial descent in wingless workers of the canopy ant *Cephalotes atratus* (Yanoviak et al., 2005). These ants exhibit a number of characteristics distinguishing them from larger vertebrate gliders, the most striking of which being that the ants lack obvious morphological adaptations for aerial behaviour. Furthermore, while most vertebrate gliders use gliding to move between physically disconnected arboreal substrata, ants only glide to escape perceived danger and to recover from accidental dislodgement from the canopy. Additionally, unlike any vertebrate glider, *C. atratus* ants glide backwards, leading with their gasters (the bulbous terminal abdominal segments) and hind-legs (Yanoviak et al., 2005).

[1]Department of Biology, University of Washington, Seattle, WA 98195, USA. [2]Department of Integrative Biology, University of California, Berkeley, CA 94720, USA. [3]Department of Biology, University of Louisville, Louisville, KY 40292, USA. [4]Smithsonian Tropical Research Institute, PO Box 2072, Balboa, Republic of Panama.

*Author for correspondence (yomunk@uw.edu)

Received 22 April 2014; Accepted 3 March 2015

Following a fall from the canopy, worker ants stabilize their body orientation, visually target a nearby tree trunk, and then glide to and land upon that tree trunk (Yanoviak and Dudley, 2006; Yanoviak et al., 2005). Surveys of gliding performance across canopy ants have revealed at least three independent origins of gliding in ants (Yanoviak et al., 2011). The ability of workers to successfully reach a target tree following ablation of the hind-limbs is significantly reduced (Yanoviak et al., 2010), suggesting that these structures are important for stabilization and control during descent.

Leaf litter studies have shown that *C. atratus* ants released at the forest floor have difficulty regaining the canopy and suffer an increased risk of attack from aggressive ant species, or fish if the ant lands in water (Yanoviak and Frederick, 2014; Yanoviak et al., 2011). For gliding to be an effective means of escaping from predators and surviving accidental falls from the canopy, gliding ants must be capable of landing on a target tree before impact with the forest floor. Therefore, the ecologically relevant aspects of aerodynamic performance for arboreal ants is the ratio of net horizontal distance travelled to vertical distance fallen for the entire descent trajectory, or glide index (*sensu* Yanoviak et al., 2005).

In this study, our objective was to measure variation in glide index for trajectories of *C. atratus* ants approaching natural targets and to determine the key factors contributing to this variation. We developed three non-exclusive hypotheses regarding parameters that could influence variation in glide index: righting phase duration, glide angle and path length (Fig. 1).

Righting phase duration

Ants dropping from the canopy may not initiate their descent in an ideal postural configuration for gliding, especially given that ants employ gliding as an escape response (Yanoviak et al., 2011). Falling animals, including non-gliders, adjust their pose while falling using an aerial righting response. In falling vertebrates, the aerial righting response is an active inertial maneuver (Jusufi et al., 2008), but in small insects the righting maneuver is typically achieved by adopting an aerodynamically stable static posture and allowing the reorientation of the body to be performed by the acting aerodynamics (Jusufi et al., 2011; Ribak et al., 2013). Once the animal has stabilized its descent, it may then require additional time to visually identify a suitable target for landing upon before beginning its horizontal motion towards that target. Assuming that the gliding ants do not begin moving horizontally until they have righted and identified a target, variation in the time required for righting and target identification could potentially influence glide index, as shown in Fig. 1A. In laboratory experiments, given sufficiently high resolution video data, righting phase duration can be estimated by directly observing body pose (Meresman et al., 2014; Ribak et al., 2013). Without access to pose information, we chose a fixed short distance (0.2 m), and defined the righting phase duration for a given trajectory as the elapsed time between the initiation of descent and the point in the trajectory where the net horizontal distance traveled became greater than this fixed distance.

The Journal of Experimental Biology (2015) 218, 1393-1401 doi:10.1242/jeb.106914

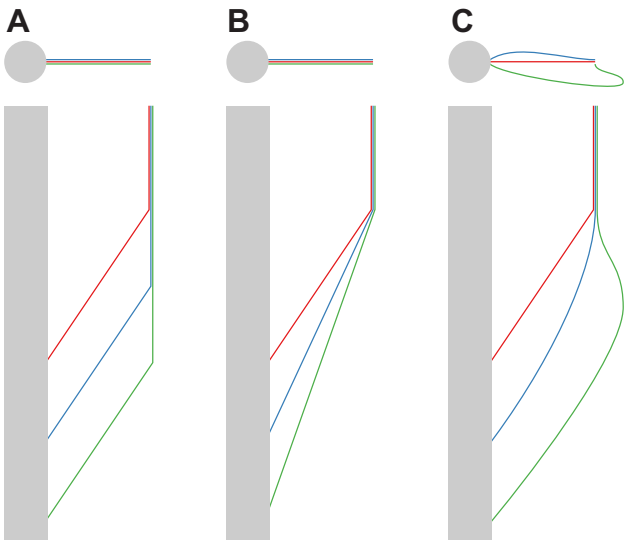

Fig. 1. Schematic diagram detailing how the glide index for a *Cephalotes atratus* ant could be influenced by three independent factors. In each case, a top view (gray circle) and side view (gray rectangle) of the target tree is provided, and three hypothetical trajectories (red, blue and green lines indicate high, middle and low glide indices). (A) Righting phase duration. (B) Glide angle. (C) Path length.

Glide angle

The instantaneous glide angle for a glider is the angle between its velocity vector and the horizontal plane, such that higher glide angles indicate steeper trajectories. If ants exhibit constant righting phase duration and follow straight paths towards their targets, but vary in the glide angles they are able to achieve, this could affect their glide index as shown in Fig. 1B. The instantaneous glide angle is given by the inverse tangent of the ratio of the vertical velocity component to the horizontal velocity component (Eqn 11). Thus, to measure glide angles from our trajectories we would require an estimate of velocity as well as position.

Path length

Ants gliding towards a target tree trunk may not necessarily travel along the most direct path available. The maneuverability of a glider represents its ability to exert active control over the aerodynamic forces acting upon it and thereby shape its trajectory; variability in the maneuverability exhibited by gliding ants may therefore determine whether ants are able to orient quickly with regard to their target and follow a direct path to their landing point, or alternatively follow a longer path. Given equal righting phase durations and glide angles, ants that follow a more circuitous path to their target will necessarily land upon their target trunk at a lower position, thereby causing variation in their glide index as shown in Fig. 1C. We chose to investigate path length as a relative quantity so that we could compare performance between trajectories. We defined relative path length as the cumulative distance traveled over the trajectory divided by the straight-line distance between the start point and the current position.

Thus, to measure these three quantities for gliding ants and quantify their influence on the glide index, we minimally needed to be able to observe 3D position and velocity. These data, in turn, allowed us to ask a secondary question concerning the role of aerodynamic equilibrium in gliding ants. Recent analyses of the trajectories of various vertebrate gliders have revealed that many gliders complete their trajectories without ever reaching equilibrium (Bahlman et al., 2013; Byrnes et al., 2008; Dudley and Yanoviak, 2011; McGuire and Dudley, 2005; Socha et al., 2010, 2005). We expected that aerodynamic equilibrium might play an important role for gliding ants, given that their wing loading and equilibrium glide speeds are comparatively low (which means that they would be expected to require less time to reach equilibrium speeds). So, in addition to our primary objectives, we set out to answer two questions regarding equilibrium gliding in ants: do gliding ants reach an equilibrium state in which the gravitational and aerodynamic forces acting upon them balance? Assuming that they do, is aerodynamic equilibrium a necessary condition for directed aerial descent?

RESULTS

We obtained two sets of 3D trajectories for ants gliding towards a target tree trunk in a natural forest setting. In the first set we collected 58 trajectories for ants dropped at a distance of 1 m from the target tree trunk (M1 group), and in the second set we obtained 13 trajectories for ants dropped 3 m from the target (M3 group). For each trajectory, we estimated 3D position and velocity at all time steps.

Kinematic determinants of glide index

In the M1 trials, the ants followed trajectories characterized by a period of near-vertical descent followed by a shallowing of glide angle and, eventually, a landing (see examples in Fig. 2). Not all ants targeted the tree trunk: in five cases, the subject targeted nearby secondary vegetation instead, including understory trees and lianas hanging from the canopy. We also observed that in at least 11 cases (15% of all trials), the ants did not successfully land on their target tree trunk with their first attempt (two examples are featured in Fig. 2). Following these unsuccessful landing attempts, the ants

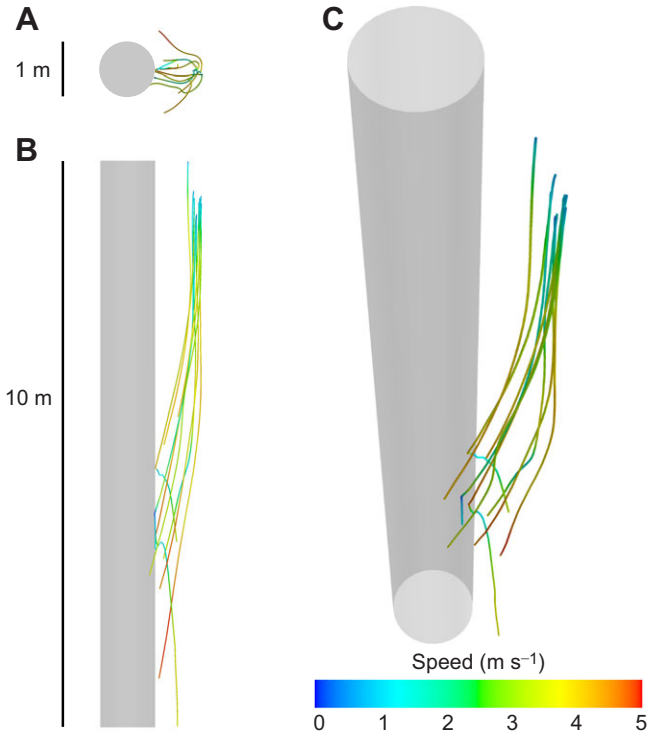

Fig. 2. A subsample of trajectories followed by gliding ants from the M1 group. Trajectories are colored according to airspeed. Gray cylinder approximately represents the target tree trunk in these rendered plots. Each trajectory represents a unique individual. (A) Top view. (B) Side view. (C) Perspective view (azimuth, 35 deg; elevation, 60 deg).

The Journal of Experimental Biology (2015) 218, 1393-1401 doi:10.1242/jeb.106914

typically bounced off the trunk, re-stabilized their descent, and returned to the target trunk for another attempt.

We derived estimates of position and velocity within all trajectories using a particle filter analysis. An example plot for a single trajectory is shown in Fig. 3. We estimated the contribution to total trajectory error from digitization errors by having seven independent and untrained digitizers each digitize the position of the ant for this trajectory. The average standard deviation in digitized pixel location was 1.23 pixels. We then recalculated the 3D trajectory for these data 100 times, injecting the digitized coordinates with a random 2D variable drawn from a Gaussian distribution centered at zero with a standard deviation of 1.23 pixels. This allowed us to characterize the 95% confidence interval for position based solely on estimated digitization errors; at the furthest point from the cameras, the 95% confidence intervals on position were 7.70 mm wide in the horizontal plane and 7.08 cm wide in the vertical direction. The shaded regions in Fig. 3 represent the total estimated error from our particle filter analysis, which naturally incorporates errors from digitization (see Materials and methods).

Glide index

To investigate variation in the glide index, we began by pooling the data from all trajectories. While the total glide index, measured between the point of release and the landing point, is the performance variable of interest, we did not expect the instantaneous glide index to remain constant throughout any given trajectory. The median trajectory exhibited little horizontal motion for approximately the first 0.5 s, increasing steadily after that time (Fig. 4A). The median net vertical travel, as expected, increased steadily from the time of release (Fig. 4B). Thus the instantaneous glide index, being the ratio of the net horizontal to vertical distance traveled from the start point, increases as the ants begin moving horizontally. After approximately 1 s, the median glide index stabilized at 0.11±0.030 (mean±s.d.). The total glide index for each trajectory was defined as the value of the instantaneous glide index at the point of first contact with the target tree trunk; as such, total glide index was computed only for those trajectories in which the trial subject successfully targeted the tree.

Righting phase duration

We defined the duration of the aerial righting phase as the time taken within the trajectory to move some fixed net horizontal distance from the point of release (0.2 m). Fig. 4A shows net horizontal motion for the pooled trajectories in our data set. The mean righting phase duration for these trajectories was 0.9±0.17 s (mean±s.d.). Fig. 5A shows righting phase duration plotted against total glide index, for all trajectories where total glide index was measured. A simple linear regression analysis revealed a significant dependence of total glide index upon righting phase duration (P<0.005, R^2=0.227).

Glide angle

Glide angle in the M1 group decreased from the point of release, indicating a shallowing of the glide angle with the progression of time (Fig. 6C). For each trajectory, following the righting phase, the mean glide angle was calculated. Across all trajectories the mean of these mean glide angles was 79.7±2.15 deg, which is consistent with previous results (Yanoviak et al., 2005). Mean post-righting glide angle is plotted against total glide index for all trajectories

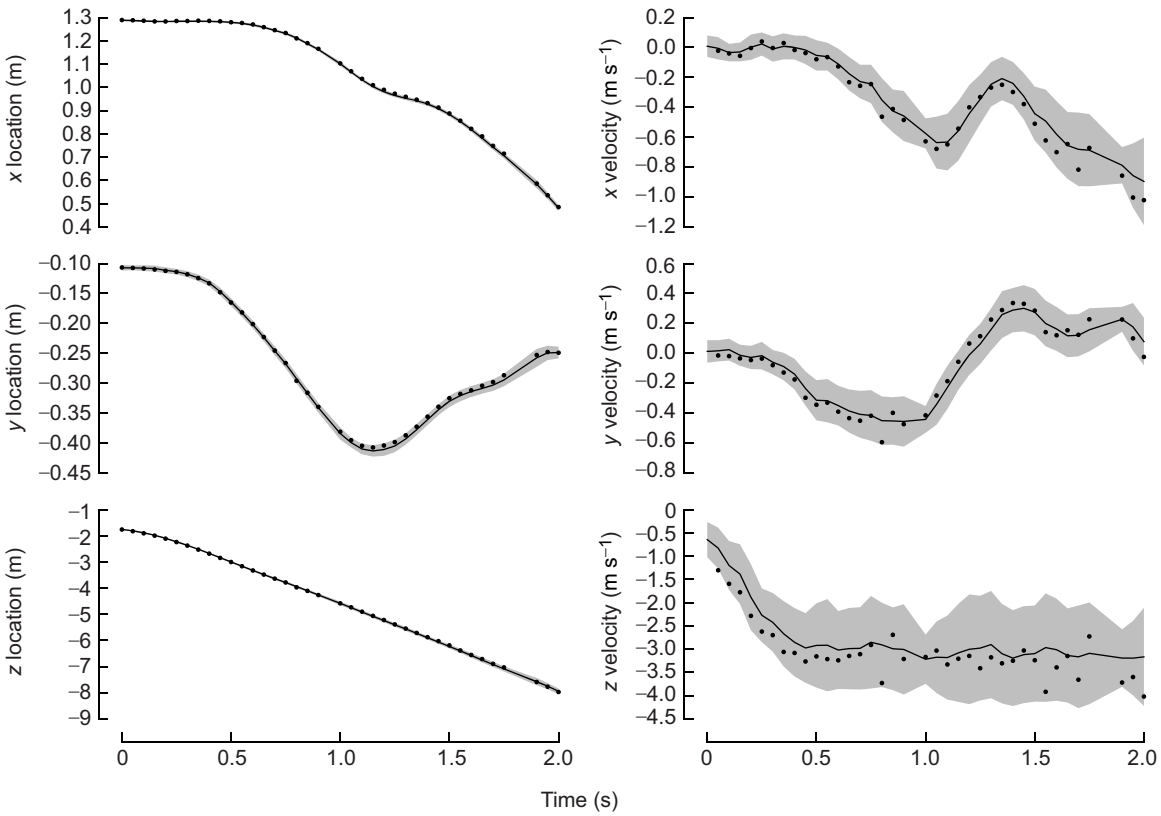

Fig. 3. Particle filter estimates of state for a single trajectory, in which the ant lands successfully on its first attempt. At each time point within the trajectory, the solid line and shaded region indicate the mean and s.d. of the state of the particles. The plotted points are the positions that 3D minimize projection error, and the velocities for these points are determined by taking the first derivative of the position data. A 3D plot of this trajectory is included in the group of trajectories plotted in Fig. 2.

The Journal of Experimental Biology (2015) 218, 1393-1401 doi:10.1242/jeb.106914

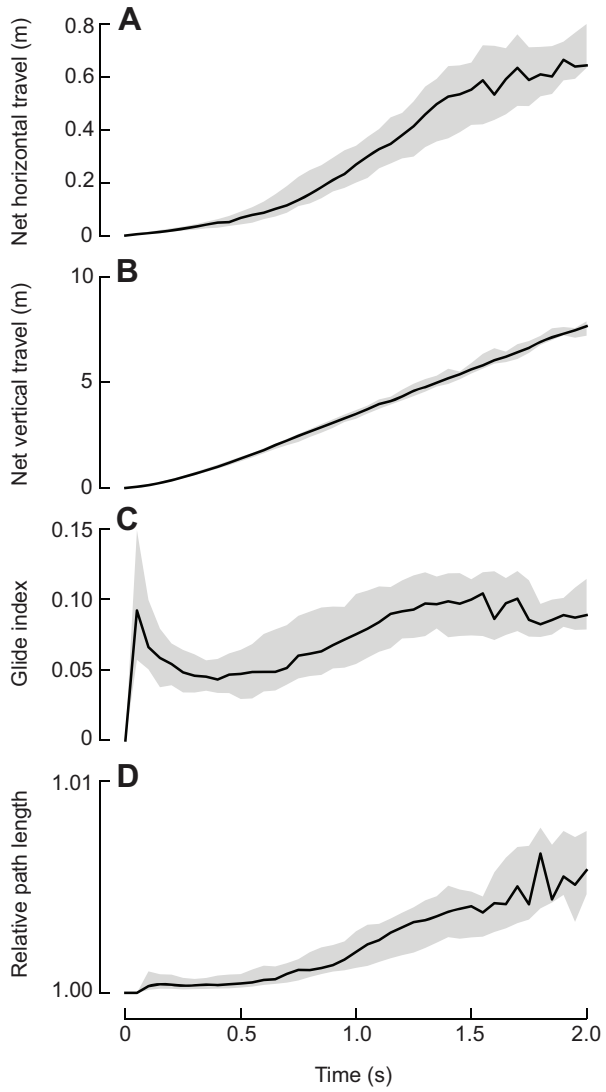

Fig. 4. Plots of net horizontal movement, vertical movement, glide index and path length for the trajectories of ants from the M1 group. In all plots, the plotted line represents the median for the group, and the shaded region indicates the inner quartiles (i.e. 50% of the trajectory data is contained within the shaded region. (A) Net horizontal distance traveled from point of release. (B) Net vertical distance traveled from point of release. (C) Glide index, defined as the ratio of the net horizontal to net vertical distance traveled. (D) Relative path length, defined as the ratio of the length of the traveled path to the length of a direct line between the current location and the point of release.

where total glide index could be measured in Fig. 5B. A simple linear regression analysis revealed a significant dependence of total glide index upon glide angle (P=0.001, R^2=0.368).

Relative path length

While the paths followed by the ants did exhibit visible curvature (see Fig. 2A), the average relative path length for trajectories was 1.0055±0.0026 (mean±s.d.; Fig. 4D). That is, the paths followed were generally less than 1% longer than a straight line path would have been. Only ants that successfully targeted and landed upon the tree were used for computing this information. For these trajectories, relative path length is plotted against the total glide index in Fig. 5C. A simple linear regression analysis revealed that the total glide index was not significantly dependent upon the relative path length (P=0.116, R^2=0.062).

Variables influencing glide index

We tested dependence of the total glide index on the righting phase duration, glide angle, relative path length and success of initial landing attempt using a multivariate linear regression analysis implemented in R (version 3.1.2) and the following model:

$$g \sim d + \theta + s + O, \quad (1)$$

where g is total glide index, d is righting phase duration, θ is glide angle, s is relative path length and O is a two-state factor describing whether the initial landing attempt was successful (that is, whether the ant stuck to the tree on first contact or bounced off). The results of our regression analysis are provided in Table 1; all variables except for success of the initial landing attempt were found to significantly affect total glide index. The multiple R^2 value for our model was 0.80, indicating that variation in total glide index is determined to a large extent by these variables. Examination of the model residuals using a normal quantile plot indicated that the residual distribution did not systematically deviate from a normal distribution.

Equilibrium gliding

Our second objective in this study was to determine the extent to which gliding ants operate in a state of aerodynamic equilibrium and, assuming that equilibrium conditions are observed, whether aerodynamic equilibrium is a prerequisite for gliding performance in ants. To answer these questions, we used our trajectory from the M1 dataset as well as the M3 trajectories, in which experimental subjects were dropped at a distance of 3 m from the target tree trunk (Fig. 7). In these M3 trials, the size and configuration of the drop volume did not allow us to include the initial part of the trajectory in the field of view of the cameras, and so these data relate only to the final approaches made by these ants towards their target tree trunk (Fig. 7). We did not observe any failed landing attempts in this group.

In the M1 group, instantaneous airspeed increased following release and steadied after approximately 1 s (Fig. 6A) to a mean value of 3.83±1.22 m s^{-1} (mean±s.d.). Instantaneous glide angle in the M1 group (Fig. 6B) begins decreasing well beforehand: that is, gliding ants in the M1 group began generating a horizontal component to their instantaneous velocity before reaching a stable airspeed. For the M3 group, where the initial phase of the descent was not recorded, the mean instantaneous airspeed was 3.57± 0.478 m s^{-1} (mean±s.d.) (Fig. 6B). Furthermore, in the M3 group, the mean instantaneous glide angle was shallower (73.0±3.61 deg) and roughly constant (Fig. 6D). A t-test confirmed that the post-righting-phase mean glide angles for the M1 and M3 groups were significantly different (P<0.005). Inspection of individual trajectories in the M3 group (Fig. 7A) show that despite the relatively stable airspeeds and glide angles observed within this group, curvature within trajectories indicates that these ants performed maneuvers to steer towards their target.

DISCUSSION

In this study, we explored three hypothetical mechanisms that could influence total glide index for gliding *C. atratus* ants, as shown in Fig. 1: righting phase duration, glide angle and path length. Our results indicate that all three factors contribute significantly to variation in observed total glide index and that collectively, these three variables account for 80% of the variation in total glide index for the trajectories that we observed. For ants in the M1 group, we observed substantial variation (0.9±0.17 s, mean±s.d.) in righting

The Journal of Experimental Biology (2015) 218, 1393-1401 doi:10.1242/jeb.106914

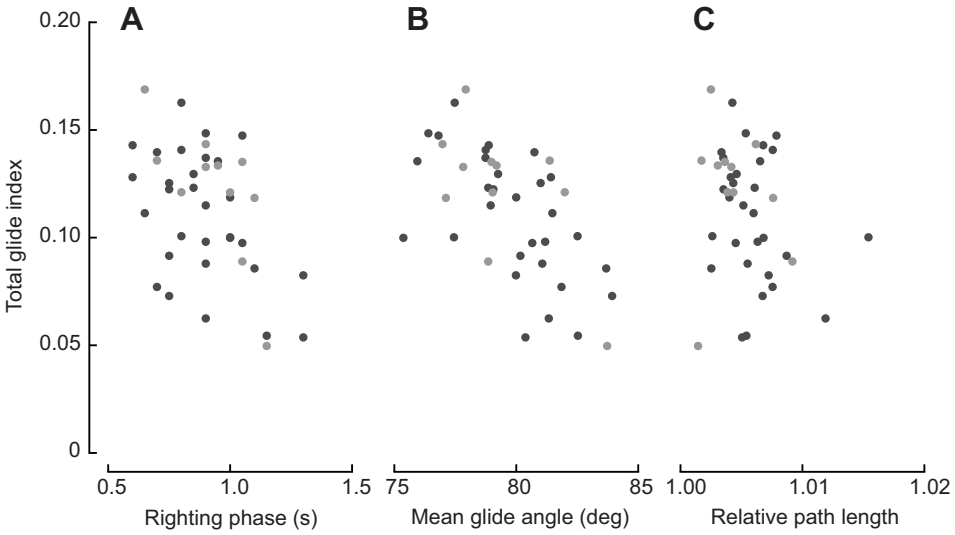

Fig. 5. Trajectories of the M1 group where the ant landed on the target tree. (A) Total glide index plotted against duration of aerial righting phase, defined as the time taken to move 0.2 m horizontally from the point of release. (B) Total glide index plotted against mean glide angle during the post-righting phase of the trajectory. (C) Total glide index plotted against relative path length, which indicates the relative difference in length between the path followed by the ant and a straight line drawn between the point of release and the point of impact. Light and dark points indicate trajectories where the initial landing attempt was unsuccessful or successful, respectively.

phase duration (Fig. 5A), and this variation significantly contributed to variation in the total glide index (t=−6.58, P≪0.001; Table 1). This variability could arise in a number of ways: gliding ants employ an aerial righting posture where the legs are elevated above the central body axis (Yanoviak et al., 2011) and so variability in the time taken by falling ants to adopt this posture and stabilize their orientation will be reflected in the time taken to initiate horizontal motion. Once stable, the ants must then visually identify their potential target and decide to initiate their approach. That five ants in the M1 group clearly failed to target the tree trunk indicates that their decision-making process may be more involved than simply selecting the largest and brightest nearby columnar object.

Following the righting phase, we observed substantial variation in mean trajectory glide angle (79.7±2.15 deg; mean±s.d., Fig. 5B). This variation in glide angle significantly contributed to variation in total glide index (t=−9.46, P≪0.001; Table 1). While we were unable to directly observe the postures employed by the gliding ants in our study, postural changes are likely to be responsible for the bulk of observed variation in the glide angle exhibited by ants (Yanoviak et al., 2010). Glide angles in the M3 group were shallower (73.1±3.61 deg) than those for the M1 group. At such steep glide angles, the small difference in mean glide angle (6.6 deg) between the M1 and M3 groups is important in determining the glide index. For gliders descending at a constant

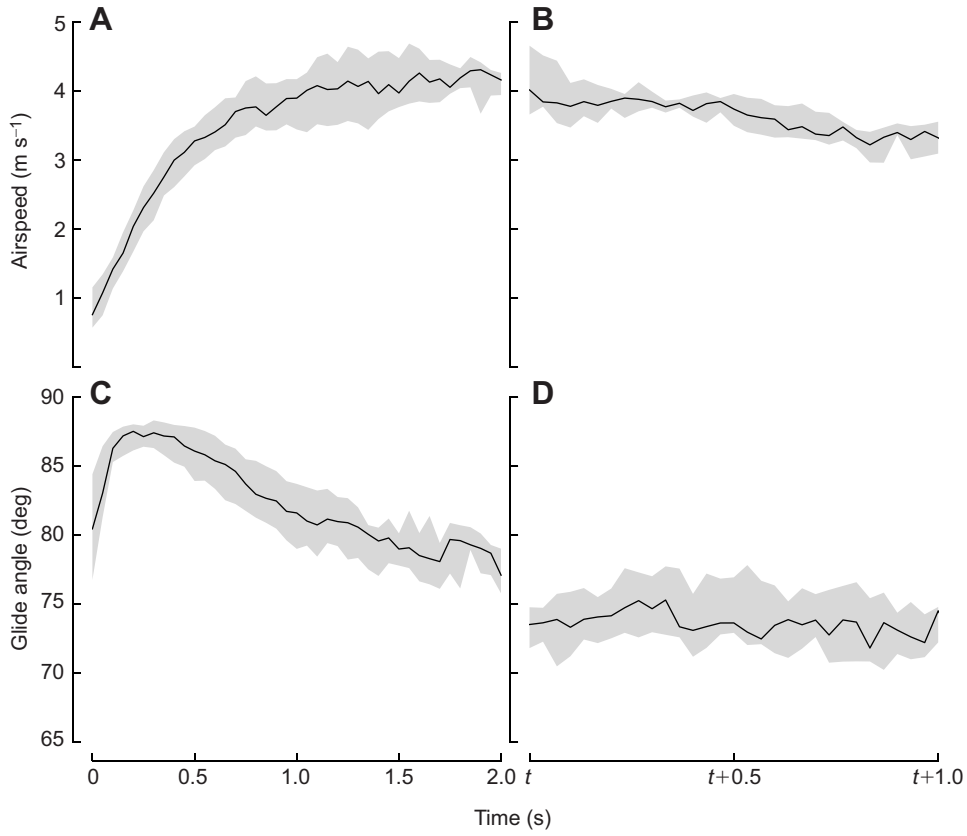

Fig. 6. Airspeed and glide angle as a function of time for M1 and M3 groups. Airspeed and glide angle in (A,C) M1 and (B, D) M3 groups of ants. As in Fig. 4, the plotted lines represent the population median, and the shaded region indicates the inner quartiles. Note that the M3 trajectories could not be aligned temporally, and so for this group time is expressed in terms of t, where t is the time of release.

The Journal of Experimental Biology (2015) 218, 1393-1401 doi:10.1242/jeb.106914

Table 1. Coefficients obtained from multiple linear regression analysis on total glide index

	Estimate	s.e.	*t* value	*P* (>|*t*|)
Intercept	5.3516	0.9619	5.56	2.66E−6
Righting phase duration (s)	−0.0858	0.0130	−6.58	1.15E−7
Mean glide angle (deg)	−0.0104	0.0011	−9.46	2.68E−11
Relative path length	−4.3020	0.9280	−4.64	4.54E−5
Initial success	−0.0043	0.0053	−0.80	0.427

Statistics computed in R (v3.1.2).

angle, the glide indices corresponding to angles of 79.7 deg and 73.1 deg would be 0.182 and 0.304, respectively: a 67% increase in glide index. The difference between the groups may either indicate that shallow glide angles require more time to develop, or that having a more-distant tree target provides an environmental cue, encouraging the adoption of more aerodynamically efficient gliding postures. While it is possible that the differences in location and camera setups for the two groups may have also affected our results, previous results indicate that *C. atratus* ants from the two regions behave similarly (Yanoviak and Dudley, 2006; Yanoviak et al., 2005).

The trajectories we measured in our study were only slightly more circuitous than a direct line path: the mean relative path length for ants in the M1 group that chose to land on the target tree was 1.005± 0.003 (mean±s.d.), indicating that trajectories were generally less than 1% longer than a straight line path from start to finish (Fig. 5C). Despite the small magnitude of variation in this parameter, our multiple linear regression indicated that relative path length contributed significantly to variability in total glide index (t=−4.64, $P \ll 0.001$; Table 1). The relatively direct nature of these trajectories indicates that gliding ants are highly maneuverable; we would expect to see more circuitous paths in gliders with a limited ability to turn.

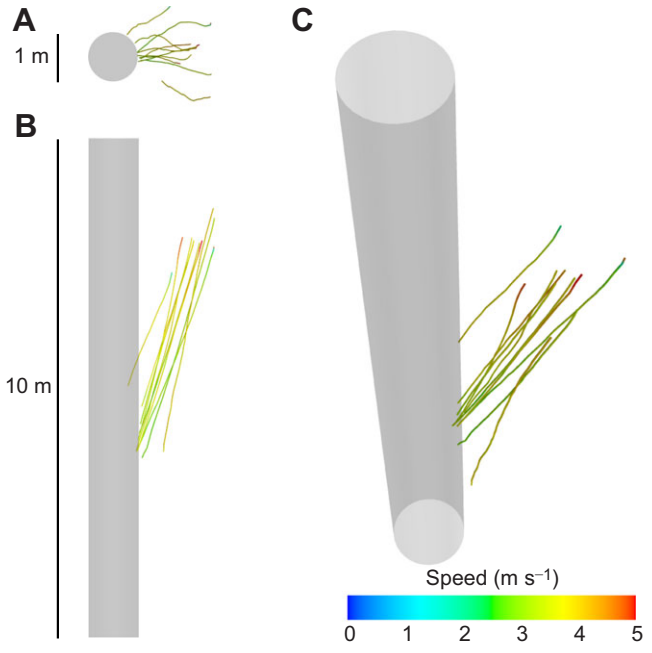

Fig. 7. Trajectories of canopy ants from the M3 group. Trajectories are colored according to airspeed. Gray cylinder approximately represents the target tree trunk in these rendered plots. Each trajectory represents a unique individual. For the M3 group, the point of release was not in view of the cameras. (A) Top view. (B) Side view. (C) Perspective view (azimuth, 35 deg; elevation, 60 deg).

Finally, our analysis allowed us to determine the extent to which ants glide at aerodynamic equilibrium. We observed that the median airspeed over the entire population of trajectories did appear to stabilize after approximately 1 s (Fig. 6). However, horizontal motion began prior to reaching stable airspeed (Fig. 6), indicating that aerodynamic equilibrium is not a prerequisite for horizontal translation in ants. After airspeeds stabilized, targeted turning maneuvers were clearly still being performed in the latter stages of the glide (e.g. Figs 2 and 7), indicating active trajectory control. Thus, while airspeeds for gliding *C. atratus* ants do quickly stabilize following the initiation of descent, *C. atratus* ants are not passive gliders and are able to disrupt the balance of forces acting on them in a controlled manner.

Overall, these wingless ant workers exhibit substantial behavioral control of flight performance given observed patterns of variation in trajectory shape and glide angle, as seen both within and among trajectories (Figs 2 and 7), which is consistent with prior results (Yanoviak et al., 2005). Control of limb posture (Yanoviak et al., 2010), as well as abdominal deflection, probably contributes to such abilities. Radical directional changes, as well as the capacity to initiate additional subsequent glides following an unsuccessful landing, are clear indicators of sophisticated aerial behavior in these and in other wingless canopy arthropods (Dudley and Yanoviak, 2011). As these mechanisms also characterize some extant apterygote gliders and may underpin the origins of flight in winged hexapods (Yanoviak et al., 2009), quantitative characterization of those axial and appendicular motions used in specific high-speed maneuvers is now warranted; high-resolution videos of stabilizing and maneuvering behavior by ants falling in a vertical wind tunnel are being used to address this issue.

MATERIALS AND METHODS

Data collection

We collected trajectory data for canopy ants (*Cephalotes atratus* Linnaeus 1758) gliding towards natural tree targets at research stations on Barro Colorado Island, Panama (Leigh, 1999), and at the Amazon Conservatory for Tropical Studies, near Iquitos, Peru (Madigosky and Vatnick, 2000) in 2008 and 2009, respectively. We obtained worker ants from local colonies by hand, using a mixture of honey and canned tuna as bait, and kept them in plastic food containers with access to sugar water for no more than 24 h before use in drop tests. We painted white dots on their dorsal surfaces to increase their visual contrast against a darker rainforest background using a paint marker. The ants were not anesthetized at any point prior to their use in experiments. In each experimental trial, we dropped a single worker ant from a height of at least 20 m near a tree trunk, and obtained video data from multiple cameras (Casio EX-F1, www.casio.com) viewing the drop volume (approximately 3×3×12 m in dimension) from different angles. In a single trial, the cameras each recorded sixty 2816×2112 pixel images in JPEG format over the course of 3 s, yielding a sampling rate of 20 Hz.

We conducted two groups of experiments: in the first group (M1), ants were dropped at a distance of 1 m horizontal from the surface of the target tree trunk, and in the second (M3) ants were dropped at a distance of 3 m horizontal.

For the M1 group, we used two cameras mounted in the canopy of the target tree trunk, separated by a distance of 2 m. In each M1 trial, one of us (Y.M.) hung from a branch in the canopy in a seated arborist harness and held the subject by its thoracic region with forceps prior to its release. For the M3 group, we used four cameras mounted on canopy platforms in trees adjacent to the target tree (Fig. 8A). In the M3 experiments, we released the ants from plastic vials internally dusted with fluorescent powder to prevent the ants from adhering to the container walls, as described by Yanoviak and Dudley (2006). Experiments were carried out in negligible wind conditions, which we assessed by confirming that nearby leafy foliage was not being visibly disturbed by wind. We did not attempt to recapture ants that returned to the tree trunk, although in many cases we did

The Journal of Experimental Biology (2015) 218, 1393-1401 doi:10.1242/jeb.106914

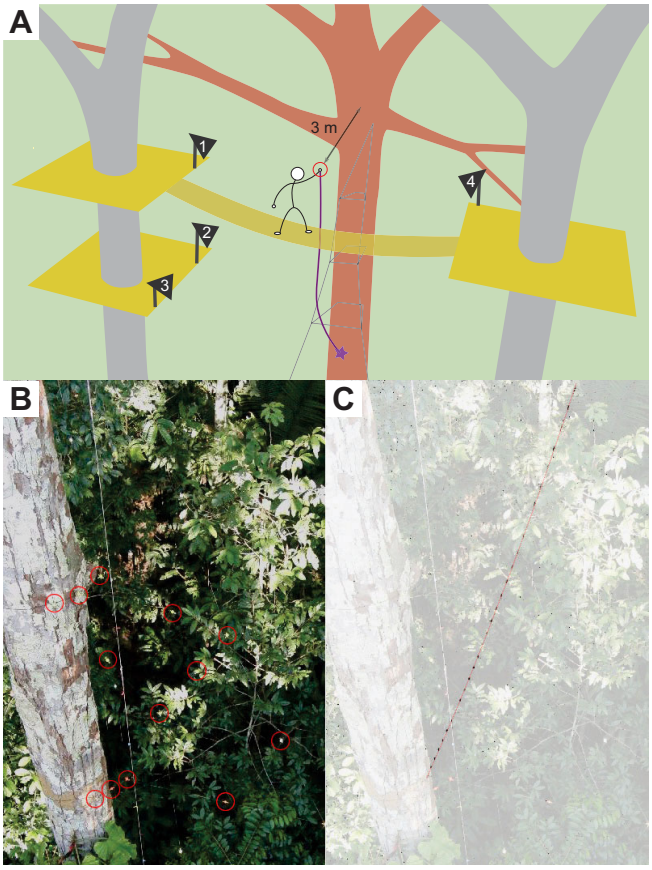

Fig. 8. Arrangement of cameras for collection of trajectories in the M3 group. (A) Cameras (represented as numbered triangles) were installed on canopy walkway platforms in trees adjacent to the target tree. A 3D calibration frame was installed in the target tree to allow for spatial calibration of the cameras. Ants were dropped from the canopy walkway at a distance of 3 m from the target tree trunk. (B) Cropped frame from one view of the target trunk, showing complex rainforest background. Markers on calibration frame are circled in red. (C) Sequence of superimposed background-subtracted images showing the position of a gliding *C. atratus* ant as it approaches the target tree trunk for a landing. The image from B is layered underneath this sequence at 20% opacity to provide a position reference.

observe experimental subjects climbing back up into the canopy following their trials.

We spatially calibrated the cameras using a 3D calibration frame attached to the target tree, which we formed using a pair of tensioned thin nylon cords stretched from the tree canopy to the forest floor, with additional cross-tensioned lines added to produce a pyramid structure (Fig. 8A,B). We measured the 3D locations of markers attached to this structure using a laser rangefinder (Leica Disto D5): the distances from each marker to each of three vantage points were measured to within 0.1 mm, and these three sets of measurements were used to triangulate the locations in 3D space of each of the markers. We then used these marker locations to define a global coordinate system and estimate projection matrices for each of the cameras using OpenCV (v2.4.9, www.opencv.org). These projection matrices define the projective transform between homogeneous image coordinates and world coordinates, analogous to the projection matrix obtained using the DLT method (Abdel-Aziz and Karara, 1971; Hartley and Zisserman, 2004; Hedrick, 2008). We then refined these estimates of our camera calibrations using the sparse bundle adjustment code developed by Lourakis and Argyros (2009) [libsba, v1.6; see also Hartley and Zisserman (2004) for a textbook treatment and Theriault et al. (2014) for applications to biological data sets].

In our experiments, we used consumer video cameras lacking a hardware frame synchronization feature and we therefore synchronized our cameras by modifying the wired external remote triggers provided and using a single button switch to control the triggering of all cameras in the rig. For the M1 group, the two cameras used were sufficiently close to one another that we were able to wire the cameras together without long cable runs. For the M3 group, the separation between the cameras was much larger, and so we used a custom wireless triggering setup using Arduino microcontrollers and XBee wireless radios to trigger the four cameras using a single remote control. In all cases, to minimize any lag between the shutter release and recording of images, the exposure and focus settings of all cameras in the rig were set manually. We later checked the synchronization of frames from each camera by looking for short-duration events (e.g. the opening of the forceps holding the subject in the M1 trials) in each image sequence and confirming that these events were aligned across all sequences.

Prior to digitizing the ant trajectories, we subtracted the relatively static rainforest background from the videos using sequential frame differencing (see Fig. 8B,C; supplementary material Movie 1). By subtracting each video frame from the frame immediately preceding it, only the pixels representing moving objects remained. We then manually digitized the position of the subject ant in each frame of each view using ImageJ (v1.48) and the MTrackJ plugin (v1.5.0). To estimate digitization errors, we followed the methods designed by Bahlman et al. (2013): for a single trajectory, seven trained individuals digitized the position of the ant in each frame and then measured the mean spread of the digitized pixel locations. The mean spread that we found according to this process was 1.23 pixels, which we used in our later analysis as the confidence in our digitization accuracy.

Trajectory estimation

Our next step was to infer the 3D trajectories followed by gliding ants using the digitized coordinates obtained from our video data. For each trial in our dataset, we first used a Monte-Carlo brute force optimization process for each set of frames corresponding to a single time point to find the 3D point which, when projected into the image planes of all available cameras, minimized the sum of the pixel distances between the projected location and the digitized coordinates. This formed our reference trajectory for our ensuing analysis. In the absence of digitization errors, this reference trajectory would be sufficient to determine the state of the ant as a function of time. However, errors in the digitization process would be expected to lead to inaccurate estimates of ant position and these errors would be amplified during estimation of velocity from differentiated position data. To obtain an accurate measurement of the position and velocity of the ants in our study in the context of these potential reconstruction errors, we modeled the gliding ants as dynamical systems and used a particle filter analysis to provide estimates of those system states.

The particle filter is a numerical method for state space estimation that is especially useful in cases where the underlying system dynamics and measurement functions are expected to have a significant non-linear component. Particle filters provide a Bayesian framework for estimating the state of a dynamical system in light of a model of the system dynamics and noisy measurements, providing an optimal estimate of the system state that minimizes model error and measurement error (Doucet and Johansen, 2009; Gordon et al., 1993; Simon, 2006).

At each time step, a population of particles is used to represent hypotheses regarding the current true state of the system based on the best estimates of the system state at the preceding time step. The particles are propagated according to the model of the system dynamics, with some random variation provided by noise; this noise generates model error, or deviations from the expected evolution of the system dynamics. These particles are then individually observed, which accounts for the fact that system state is often not directly measurable but must be inferred using some intermediate instrument; in the example of camera-based trajectory analysis, 3D positions are not directly observed, but are inferred using multiple 2D projections onto the imaging planes of synchronized cameras. These observations are compared with the actual measurements and the discrepancy between the particle observations and the actual measurement provides a second error estimate, the measurement error. The model error and measurement error are now combined, with their proportionate weightings dependent on the relative and subjective degree of confidence afforded to the model and the measurements, to provide a weight for each particle. The normalized

The Journal of Experimental Biology (2015) 218, 1393-1401 doi:10.1242/jeb.106914

distribution of these particle weights forms a probability density function representing the confidence that the state of any given particle reflects the true state of the system. A new population of particles is then drawn from this probability density function, and the process then continues with these particles being projected forward into the next time step according to the system model.

In our case, we performed our particle filter analysis using a linear state model, where the state of the system at some time t consists of its 3D position $\mathbf{x}$ and velocity $\dot{\mathbf{x}}$:

$$\begin{aligned}\mathbf{x}(t) &= \mathbf{x}(t-1) + \dot{\mathbf{x}}(t-1)\Delta t + \mathbf{w},\\ \dot{\mathbf{x}}(t) &= \frac{\mathbf{x}(t) - \mathbf{x}(t-1)}{\Delta t},\end{aligned} \tag{2}$$

where t and $t-1$ denote two successive points in time for which measurements of the system are available, with Δt being the elapsed time between those measurements, and $\mathbf{w}$ is a Gaussian noise variable. In most cases, we expected that Eqn 2 would roughly hold. However, we also knew that the ants would occasionally collide with solid substrates and bounce off in a new direction: in these cases, the model of Eqn 2 would provide a poor estimate of the new state of the ant after collision. We therefore included a second model covering our expectations regarding what would happen to the ant as it bounced off a solid surface. Assuming inelastic collisions, we modeled the system dynamics as follows:

$$\begin{aligned}\mathbf{x}(t) &= \mathbf{x}(t-1) + \mathbf{w},\\ \dot{\mathbf{x}}(t) &= \frac{\mathbf{x}(\mathrm{t}) - \mathbf{x}(\mathrm{t}-1)}{\Delta t}.\end{aligned} \tag{3}$$

The measurement model, $\mathbf{y}_t = f(\mathbf{x}_t)$, is given by the camera calibrations, such that $\mathbf{y}_t$ contains the digitized pixel locations of the ant in each available frame for time t, and the function f describes the projective transform for each camera from 3D world coordinates to image coordinates.

At the beginning of each M1 trajectory, we generated 1000 particles localized around the reference trajectory ant position, smearing the positions of these particles with a Gaussian function to inject noise into the particle population. As the ants in the M1 group were being tracked from their point of release, their initial velocity was set to zero plus some Gaussian noise ($\sigma_{\dot{x}}$=0.05, $\sigma_{\dot{y}}$=0.05, $\sigma_{\dot{z}}$=0.1). All of the noise values for the z direction were given a negative sign, based on the assumption that ants would be unlikely to have an initial upwards velocity.

These particles composed a set of 1000 independent hypotheses regarding the true state of the ant. We evaluated the likelihood of each of these hypotheses by using our camera calibration models to project their positions in 3D space onto the image planes of the cameras and comparing the pixel locations of the projected particles to the actual measurement location:

$$e_{\mathrm{proj}} = \sum_{\mathrm{cam}} \sqrt{(u_{\mathrm{proj}} - u_{\mathrm{meas}})^2 + (v_{\mathrm{proj}} - v_{\mathrm{meas}})^2}, \tag{4}$$

where, for a given camera frame, (u_{meas}, v_{meas}) is the digitized pixel location and (u_{proj}, v_{proj}) is the projected pixel location of the particle. The sum of these discrepancies in pixel location over all cameras is e_{proj}, the measurement error.

We compared the projection errors for the population of particles to the projection error for the reference trajectory, and assigned a weight value to each particle using a Gaussian probability density function with a standard deviation equal to the reference projection error (representing the minimum achievable reconstruction error). The minimum standard deviation we used in this weighting process was 1.23 times the number of cameras (2.43 for the M1 group, 4.94 for the M3 group) to account for digitizing errors (see previous section). Using this weighting function, particles with projection errors close to the reference projection error were assigned higher weights.

We then computed a model error for each particle using:

$$e_{\mathrm{model}} = \frac{|\dot{\mathbf{x}}(t) - \dot{\mathbf{x}}(t-1)|}{|\dot{\mathbf{x}}(t)|}, \tag{5}$$

where $\dot{\mathbf{x}}(t)$ represents the velocity component of the state at time t. Thus, the model error (e_{model}) is the relative change in velocity between two successive time steps, and will be minimized when the velocity does not change between time steps. We computed a set of weights based on model error using a Gaussian probability density function centered about zero with a standard deviation of 0.05, indicating our expectation that changes in velocity between successive time steps (i.e. 0.05 s) should be small.

Finally, we normalized both weight vectors to sum to 0.5, and then added the weights together to obtain a normalized posterior probability distribution of the likelihood that any given particle represented the true state of the descending ant. We then performed a resampling step, drawing a new set of 1000 particles from the weighted posterior distribution, so that the states associated with the most highly weighted particles would be disproportionately well represented in the resampled distribution. This new set of particles was then propagated forward according to our system dynamics models. For each particle, a system model was randomly assigned (95% of particles were propagated according to Eqn 2, the remaining 5% according to Eqn 3) and the state of the particle was updated according to that model. These particle states were then compared with the measurement data for the next set of image frames in the sequence, and this process then continued until the end of the trajectory was reached.

When we reached the end of the available measurements for a given trajectory, we were left with a trajectory composed of 1000 particle states at each time step, distributed according to the probability density function obtained from our weighting scheme. We then took the mean of those particle states at each time step to arrive at our estimate of the trajectory, and used the standard deviation of those particle states to estimate the error in our trajectories.

Computation of gliding metrics

To test our hypotheses regarding factors potentially affecting total glide index, we computed net horizontal travel [$d_{\mathrm{h}}(t)$], net vertical travel [$d_{\mathrm{v}}(t)$], instantaneous glide index [$g(t)$], relative path length [$s(t)$], air speed [$v(t)$] and instantaneous glide angle [$\theta(t)$] for each trajectory as a function of time:

$$d_{\mathrm{h}}(t) = |\mathbf{x}_{xy}(t) - \mathbf{x}_{xy}(0)|, \tag{6}$$

$$d_{\mathrm{v}}(t) = |\mathbf{x}_{z}(t) - \mathbf{x}_{z}(0)|, \tag{7}$$

$$g(t) = \frac{d_{\mathrm{h}}(t)}{d_{\mathrm{v}}(t)}, \tag{8}$$

$$s(t) = \frac{\sum_1^t |\mathbf{x}(t) - \mathbf{x}(t-1)|}{|\mathbf{x}(t) - \mathbf{x}(0)|}, \tag{9}$$

$$v(t) = |\dot{\mathbf{x}}(t)|, \tag{10}$$

$$\theta(t) = \tan^{-1}\left(\frac{|\dot{\mathbf{x}}_z(t)|}{|\dot{\mathbf{x}}_{xy}(t)|}\right), \tag{11}$$

where $\mathbf{x}_{xy}$ is a 2-vector representing the x and y coordinates and $\mathbf{x}_z$ is the z-coordinate. As the measurements for the M3 group did not include the point of release, only $v(t)$ and $\theta(t)$ were computed for these trajectories.

Having computed these values for all trajectories, we then pooled all of the data in each group by t, allowing us to inspect the distribution of these values as a function of the time elapsed following the initiation of descent. This pooled data set allowed us to compute the distribution of total glide index, righting phase duration, glide angle and relative path length across all trajectories in our data set.

Acknowledgements

Feedback from two anonymous reviewers greatly improved this manuscript from an earlier version; in particular, the particle filter analysis described here was developed in response to insightful comments from the second reviewer. Tyson Read assisted with gathering trajectory data for the M1 group. We thank Oris Acevedo, Pam Bucur, Stephen Madigosky and Belkys Jimenez for logistical support. The Smithsonian Tropical Research Institute, the Panamanian Autoridad Nacional del Ambiente (ANAM) and the Peruvian Instituto Nacional de Recursos Naturales (INRENA) provided research permits. The Smithsonian Tropical Research Institute and the Amazon Conservatory for Tropical Studies facilitated access to field sites in Panama and Peru.

Competing interests
The authors declare no competing or financial interests.

Author contributions
Y.M. designed and executed the experiments, and performed all data analyses with advice from S.P.Y., M.A.R.K. and R.D. Y.M., S.P.Y., M.A.R.K. and R.D. drafted and revised the manuscript.

Funding
This research was supported by grants from the National Science Foundation (IOS-0837866 to R.D. and IOS-0843120 to S.P.Y.), and the Virginia G. and Robert E. Gill Chair to M.A.R.K.

Supplementary material
Supplementary material available online at
http://jeb.biologists.org/lookup/suppl/doi:10.1242/jeb.106914/-/DC1

References

Abdel-Aziz, Y. and Karara, H. (1971). Direct linear transformation from comparator coordinates in close-range photogrammetry. In *Proc. Symp. on Close-Range Photogrammetry*, pp. 1-18. University of Chicago at Urbana-Champaign.
Bahlman, J. W., Swartz, S. M., Riskin, D. K. and Breuer, K. S. (2013). Glide performance and aerodynamics of non-equilibrium glides in northern flying squirrels (*Glaucomys sabrinus*). *J. R. Soc. Interface* **10**, 20120794.
Bishop, K. (2006). The relationship between 3-d kinematics and gliding performance in the southern flying squirrel, *Glaucomys volans*. *J. Exp. Biol.* **209**, 689-701.
Byrnes, G., Lim, N. T.-L. and Spence, A. J. (2008). Take-off and landing kinetics of a free-ranging gliding mammal, the malayan colugo (*Galeopterus variegatus*). *Proc. R. Soc. B Biol. Sci.* **275**, 1007-1013.
Doucet, A. and Johansen, A. M. (2009). A tutorial on particle filtering and smoothing: fifteen years later. In *Oxford Handbook of Nonlinear Filtering*, Vol. 12 (ed. D. Crisan and B. Rozovskii), pp. 656-704. Oxford: Oxford University Press.
Dudley, R. and Yanoviak, S. P. (2011). Animal aloft: the origins of aerial behavior and flight. *Integr. Comp. Biol.* **51**, 926-936.
Dudley, R., Byrnes, G., Yanoviak, S. P., Borrell, B., Brown, R. M. and McGuire, J. A. (2007). Gliding and the functional origins of flight: biomechanical novelty or necessity? *Annu. Rev. Ecol. Evol. Syst.* **38**, 179-201.
Emerson, S. B. and Koehl, M. A. R. (1990). The interaction of behavioral and morphological change in the evolution of a novel locomotor type: “flying” frogs. *Evolution* **44**, 1931-1946.
Gordon, N. J., Salmond, D. J. and Smith, A. F. M. (1993). Novel approach to nonlinear/non-Gaussian Bayesian state estimation. *IEE Proc. F* **140**, 107-113.
Hartley, R. and Zisserman, A. (2004). *Multiple View Geometry in Computer Vision*, 2nd edn. Cambridge: Cambridge University Press.
Hedrick, T. L. (2008). Software techniques for two- and three-dimensional kinematic measurements of biological and biomimetic systems. *Bioinspir. Biomim.* **3**, 034001.
Jusufi, A., Goldman, D. I., Revzen, S. and Full, R. J. (2008). Active tails enhance arboreal acrobatics in geckos. *Proc. Natl. Acad. Sci. USA* **105**, 4215-4219.
Jusufi, A., Zeng, Y., Full, R. J. and Dudley, R. (2011). Aerial righting reflexes in flightless animals. *Int. Comp. Biol.* **51**, 937-943.
Kingsolver, J. G. and Koehl, M. A. R. (1994). Selective factors in the evolution of insect wings. *Annu. Rev. Entomol.* **39**, 425-451.
Leigh, E. (1999). *Tropical Forest Ecology: A View from Barro Colorado Island*. Oxford University Press.
Lourakis, M. I. A. and Argyros, A. A. (2009). Sba: a software package for generic sparse bundle adjustment. *ACM Trans. Math. Software* **36**, 1-30.
Madigosky, S. R. and Vatnick, I. (2000). Microclimatic characteristics of a primary tropical Amazonian rain forest, ACEER, Iquitos, Peru. *Selbyana* **21**, 165-172.
McCay, M. G. (2001). Aerodynamic stability and maneuverability of the gliding frog *Polypedates dennysi*. *J. Exp. Biol.* **204**, 2817-2826.
McGuire, J. A. (2003). Allometric prediction of locomotor performance: an example from Southeast Asian flying lizards. *Am. Nat.* **161**, 337-349.
McGuire, J. A. and Dudley, R. (2005). The cost of living large: comparative gliding performance in flying lizards (Agamidae: *Draco*). *Am. Nat.* **166**, 93-106.
Meresman, Y., Ribak, G., Weihs, D. and Inbar, M. (2014). The stimuli evoking the aerial-righting posture of falling pea aphids. *J. Exp. Biol.* **217**, 3504-3511.
Ribak, G., Gish, M., Weihs, D. and Inbar, M. (2013). Adaptive aerial righting during the escape dropping of wingless pea aphids. *Curr. Biol.* **23**, R102-R103.
Simon, D. (2006). *Optimal State Estimation: Kalman, H-infinity, and Nonlinear Approaches*. Hoboken, NJ, USA: Wiley-Interscience.
Socha, J. J., O’Dempsey, T. and LaBarbera, M. (2005). A 3-d kinematic analysis of gliding in a flying snake, *Chrysopelea paradisi*. *J. Exp. Biol.* **208**, 1817-1833.
Socha, J. J., Miklasz, K., Jafari, F. and Vlachos, P. P. (2010). Non-equilibrium trajectory dynamics and the kinematics of gliding in a flying snake. *Bioinspir. Biomim.* **5**, 045002.
Theriault, D. H., Fuller, N. W., Jackson, B. E., Bluhm, E., Evangelista, D., Wu, Z., Betke, M. and Hedrick, T. (2014). A protocol and calibration method for accurate multi-camera field videography. *J. Exp. Biol.* **217**, 1843-1848.
Yanoviak, S. P. and Dudley, R. (2006). The role of visual cues in directed aerial descent of *Cephalotes atratus* workers (Hymenoptera: Formicidae). *J. Exp. Biol.* **209**, 1777-1783.
Yanoviak, S. P. and Frederick, D. N. (2014). Water surface locomotion in tropical canopy ants. *J. Exp. Biol.* **217**, 2163-2170.
Yanoviak, S. P., Dudley, R. and Kaspari, M. (2005). Directed aerial descent in canopy ants. *Nature* **433**, 624-626.
Yanoviak, S. P., Kaspari, M. and Dudley, R. (2009). Gliding hexapods and the origins of insect aerial behaviour. *Biol. Lett.* **5**, 510-512.
Yanoviak, S. P., Munk, Y., Kaspari, M. and Dudley, R. (2010). Aerial manoeuvrability in wingless gliding ants (*Cephalotes atratus*). *Proc. R. Soc. B Biol. Sci.* **277**, 2199-2204.
Yanoviak, S. P., Munk, Y. and Dudley, R. (2011). Evolution and ecology of directed aerial descent in arboreal ants. *Int. Comp. Biol.* **51**, 944-956.
Young, B. A., Lee, C. E. and Daley, K. M. (2002). On a flap and a foot: aerial locomotion in the “flying” gecko, *Ptychozoon kuhli*. *J. Herp.* **36**, 412-418.